

SUPPORTING INFORMATION to

Model Building Analysis - a novel method for statistical evaluation of Pt L3-edge EXAFS data to unravel the structure of Pt-alloy nanoparticles for the oxygen reduction reaction on highly oriented pyrolytic graphite.

Felix E. Feiten¹, Yuki Wakisaka¹, Shuntaro Takahashi², Naoto Todoroki², Toshimasa Wadayama², Oki Sekizawa^{3,4}, Tomohiro Sakata³, Tomoya Uruga^{3,4}, Yasuhiro Iwasawa³, Kiyotaka Asakura^{1,}*

¹Institute for Catalysis, Hokkaido University, Hokkaido, Japan

²Graduate School of Environmental Studies, Tohoku University, Sendai, Japan

³Innovation Research Center for Fuel Cells, University of Electro-Communications, Tokyo, Japan

⁴Japan Synchrotron Radiation Research Institute (JASRI), Hyogo, Japan

Page 3	Figure S1. Electrochemical cell used in the EXAFS experiments Explanation of spikes in the experimental EXAFS spectra
Pages 4	Figure S2. Averaged Pt LIII-edge EXAFS data for all samples.
Page 5	Figures S3 to S8. STEM images of the NP samples
Page 6	Figure S9. Demonstration of the edge jump determination
Pages 6-8	Discussion of statistical significance of the third decimal digit in the bond lengths determined by EXAFS analysis
Pages 8-9	Error estimation for $r(\text{Pt-Pt})$ and $r(\text{Pt-Co})$ and correlation between r and ΔE_0 (Figure S10)
Pages 9-10	Correlation between N and σ^2 (Figure S11)
Pages 10-12	2D Mapping and Filtering
Pages 13-21	Figures S12 to S62. Contour plots showing the results of 2D Mapping and Filtering
Pages 21-22	Additional explanations about the computer program used to generate the structural models for the nanoparticles
Page 23	Table S1. Minimum and maximum Pt/Co-ratios used in the model building, numbers of structural models and numbers of comparisons between structural models and EXAFS fits before and after filtering as well as resulting numbers of EXAFS fits
Page 24	Figures S63 to S66. EXAFS fit parameters for simple EXAFS and Model Building Analysis with Error Bars.
Page 25	Table S2. Overview over EXAFS parameters resulting from the filtered model building comparisons
Page 26	Figure S67. Correlation between area specific activity and Pt-Pt bond distances of Pt M alloy particles on C powder prepared in the previously reported way and those on HOPG prepared by APD method (this work).

Electrochemical cell used in the EXAFS experiments

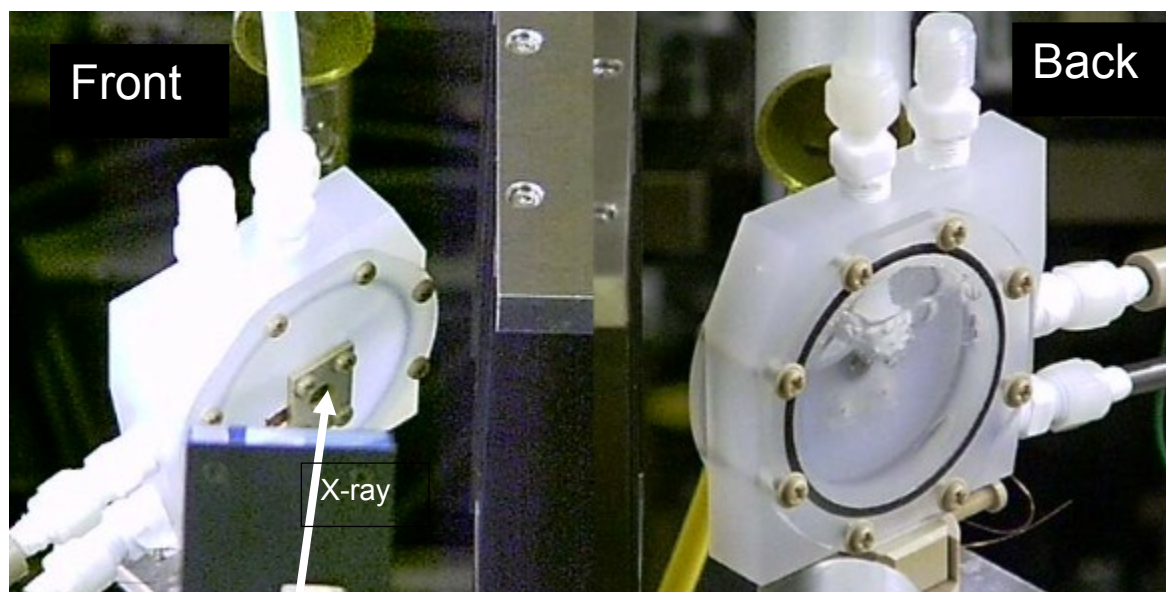


Figure S1. Electrochemical cell used in the EXAFS experiments

Explanation of spikes in the experimental EXAFS spectra

The raw EXAFS spectra contain many spikes. The origin of these spikes is not entirely clear. They are not glitches caused by multiple diffractions in the monochromator, because the spikes occurred randomly. The spikes occur when large bubbles desorb from the working electrode (the sample) and therefore we think this process is the origin of the spikes. The bubbles were not created by the applied potential but by X-ray illumination of the solution, i.e. they also appear without an applied potential as long as X-rays are hitting the sample and solution. Thus we conclude that X-ray induced water splitting creates the bubbles. During X-ray illumination, the bubbles gradually grow and are detached from the electrode at a certain size. At this moment, the bubble is completely removed but a new bubble starts forming immediately. The measured X-ray signal changes at the moment of desorption of a bubble due to the intensity change of inelastic scattering X-ray from the solution at the same energy of fluorescence X-ray, resulting in a spike in the spectrum.

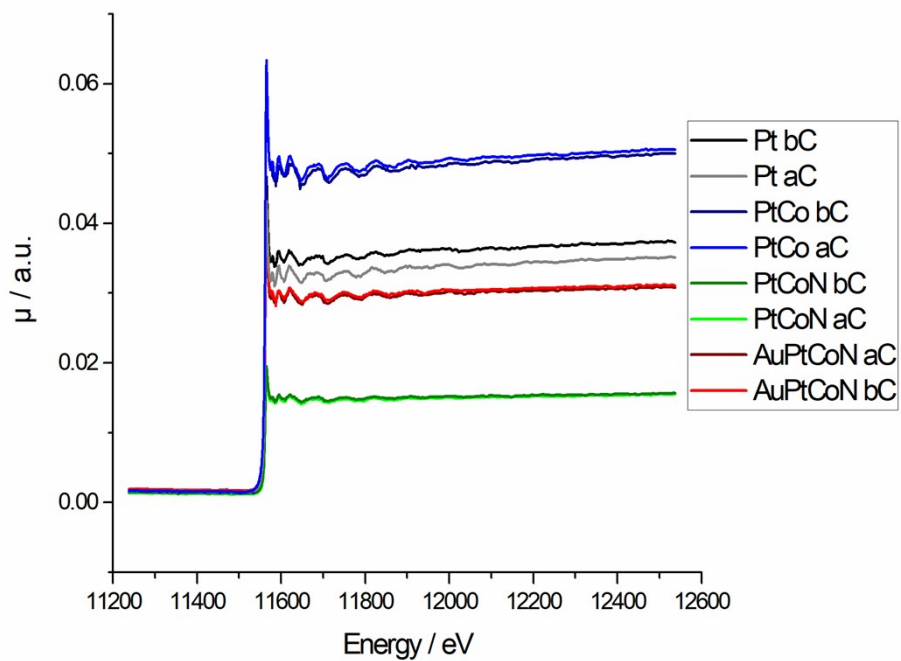


Figure S2. Averaged Pt L_{III}-edge EXAFS data. The average of the deglitched spectra for all 5 scans (3 scans for PtCoN after conditioning, 4 scans for AuPtCoN after conditioning) for each sample before (bC) and after (aC) conditioning is shown.

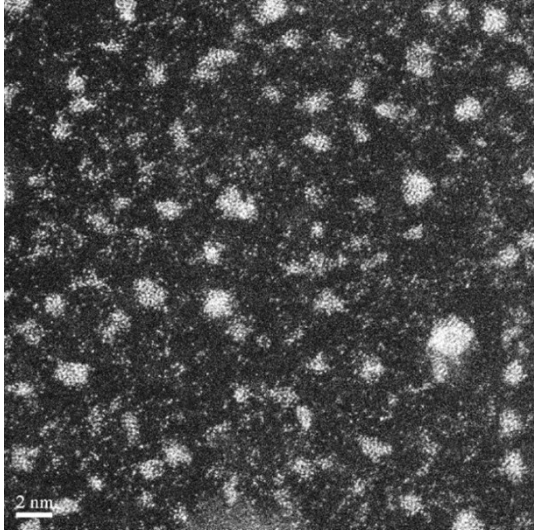


Figure S3. HAADF-STEM image of PtCo bc

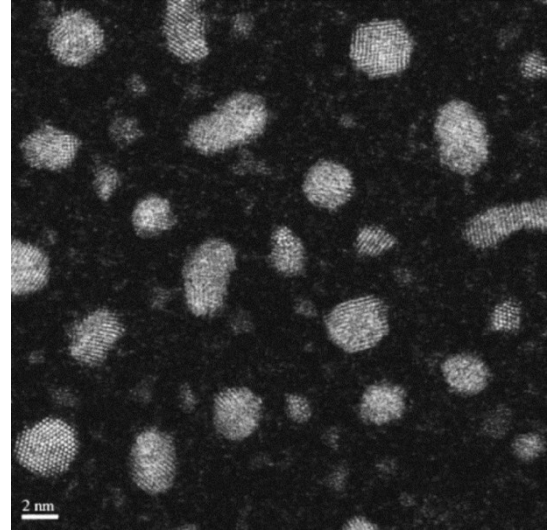


Figure S6. HAADF-STEM image of PtCoN ac

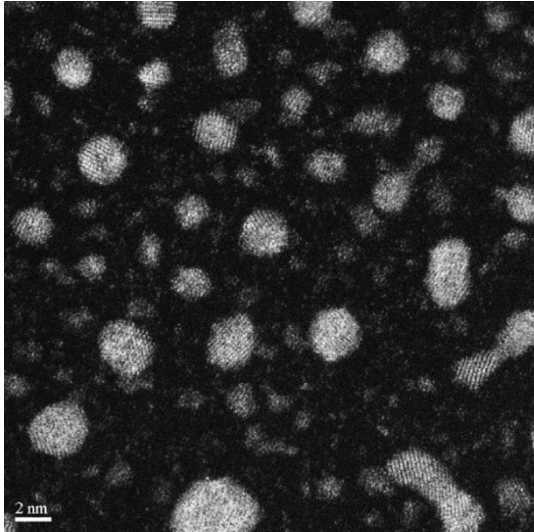


Figure S4. HAADF-STEM image of PtCo ac

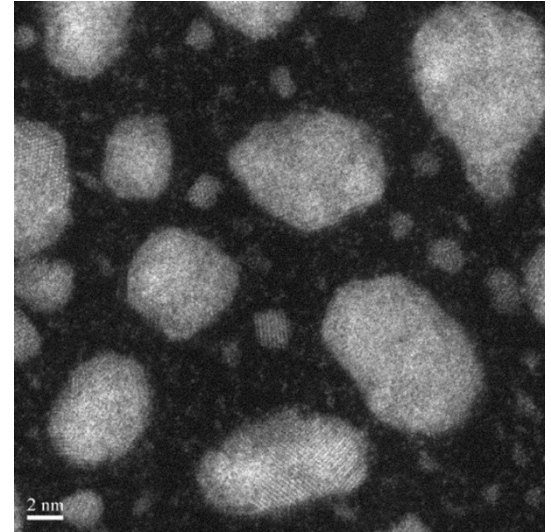


Figure S7. HAADF-STEM image, AuPtCoN bc

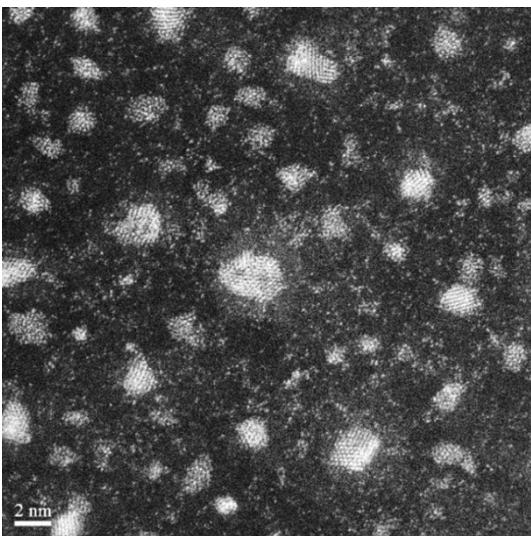


Figure S5. HAADF-STEM image of PtCoN ac

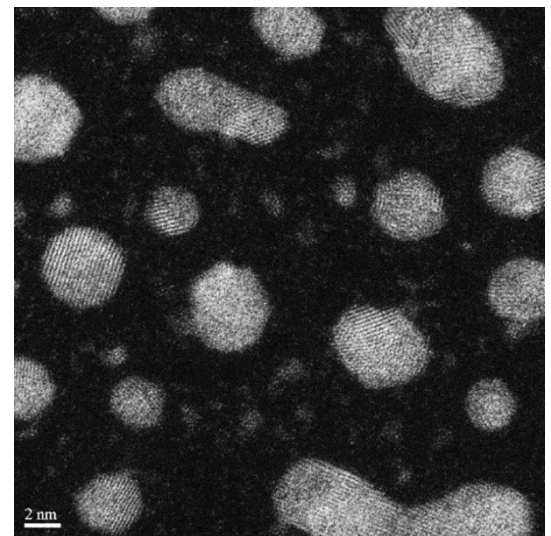


Figure S8. HAADF-STEM image, AuPtCoN ac

Edge jump analysis

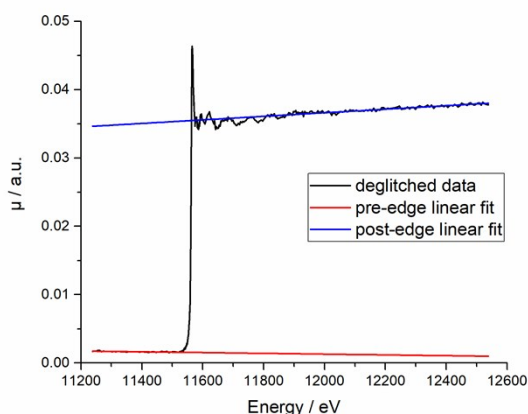


Figure S9. Demonstration of the edge jump determination on a single EXAFS scan of the Pt NPs before electrochemical conditioning.

The edge jump is determined as the difference between post-edge linear fit and pre-edge linear fit at the position of the second minimum after the maximum of the curve.

Discussion of statistical significance of the third decimal digit in the bond lengths determined by EXAFS analysis

Table 2 about EXAFS Fitting Results in the paper shows that the errors for the bond lengths determined by simple EXAFS are 0.01 Å or larger. This seems to suggest that there is no meaning to the third decimal digit of the bond lengths. In order to quantify the statistical significance of changes in the third decimal digit of the bond lengths we performed F-tests according to Hamilton [1] using the following formula proposed by Downward et al. [2]:

$$F = \left[\left(\frac{R_1}{R_0} \right)^2 - 1 \right] \frac{(n - m)}{b}$$

S1

All six fit parameters from the simple EXAFS fitting were fixed and $r(\text{Pt-Pt})$ varied in steps of 0.001 Å. The resulting R-factors R_1 were compared with the best fit R-factor R_0 using the formula above. n is the number of independent datapoints (10.3 for our measurements), m is the number of fit parameters (6) and b is the dimensionality of the hypothesis to be tested ($b=1$, since only the Pt-Pt bond length was varied in the F-test). The resulting F-values were

compared with the tables given by Hamilton in [1] to obtain the statistical significance of the change in $r(\text{Pt-Pt})$ relative to the best fit.

The F-tests indicate that changes of 0.003 Å are statistically significant with more than 90 % probability for some of the simple EXAFS fits and insignificant (less than 90 % probability of statistical significance) for others. For all fits, changes of 0.005 Å or more are statistically significant (more than 90 % probability of statistical significance). In combination with the errors obtained in the least squares fitting procedure used in the simple EXAFS this suggests that the third decimal digit in the Pt-Pt bond lengths for simple EXAFS is of limited reliability.

F-tests for the results of the model building analysis are somewhat more complicated since it is not straightforward to determine the correct value of m to use. One reasonable value could be six, as in the analysis of the simple EXAFS fits, but it could also be argued that an m value of four is more reasonable, since the two Debye Waller-factors for Pt-Pt and Pt-Co paths are kept fixed in the 2D-mapping. If $m = 6$ is used, changes in $r(\text{Pt-Pt})$ of 0.004 Å are significant (90 %-level or higher) for PtCo ac, PtCoN ac and AuPtCoN bc and insignificant (less than 90 % level) for PtCo bc, PtCoN bc and AuPtCoN ac. For $m = 4$, changes of 0.004 Å are significant for all samples except PtCo bc. Changes of 0.003 Å are only significant for PtCoN ac.

This analysis indicates that changes in the third decimal place of the Pt-Pt bond length are on the verge of being statistically relevant.

However, the error analysis for $r(\text{Pt-Pt})$ and $r(\text{Pt-Co})$, presented below, indicates that the errors are larger than 0.01 Å for all samples. Since our error estimate is very conservative, i.e. the real errors should be smaller than the error calculated by us, we use the third decimal place in $r(\text{Pt-Pt})$ and $r(\text{Pt-Co})$ in the plots comparing the bond lengths between the different samples (Figures 5 and 6 in the paper and Figures S65 and S66 in the Supporting Information). However, we only show two decimal places in Table 2 and Table S2 because of the large errors. Dealloying should lead to an increase in the Pt-Pt bond length. So the very small increases in $r(\text{Pt-Pt})$ as a result of dealloying for the PtCoN and AuPtCoN samples agree well with their relatively high structural stability.

[1] Hamilton, W. C. Significance Tests on the Crystallographic R Factor. *Acta Cryst.*, **1965**, 18, 502–510. <http://doi.org/10.1107/S0365110X65001081>

[2] Downward, L., Booth, C. H., Lukens, W. W., Bridges, F. A variation of the F-test for determining statistical relevance of particular parameters in EXAFS fits. *AIP Conference Proceedings*, 2007, 882, 129–131. <http://doi.org/10.1063/1.2644450>

Error estimation for $r(\text{Pt-Pt})$ and $r(\text{Pt-Co})$ and correlation between r and ΔE_0

The bond length, r , and the shift of the energy scale, ΔE_0 , are directly correlated in the EXAFS equation. This does not lead to the same problems as the correlation between coordination number N and Debye-Waller factor σ^2 , discussed in the paper and the next section of the Supporting Information, because we fix ΔE_0 to the value obtained on a Pt reference foil. However, errors in ΔE_0 as obtained on the reference foil as well as possible deviations in ΔE_0 over the course of the experiments do lead to a corresponding error in r which we discuss here.

Our error analysis uses the F-test described in the previous section.

We systematically varied ΔE_0 and $r(\text{Pt-Pt})$ for the Pt reference foil, while optimizing all other fit parameters, as shown in Figure S10 below. Our null hypothesis for the F-test is “Two fits are equally good even though they have different ΔE_0 and $r(\text{Pt-Pt})$ ”. Comparison of two fits then gives the statistical probability with which the null hypothesis can be rejected. This is shown with the color scale in Figure S10. We use all datapoints for which the null hypothesis can not be rejected with 95 % significance or more to calculate the error in ΔE_0 , as indicated by the white dashed lines in Figure S10. It should be noted that all datapoints at 6.75 eV and

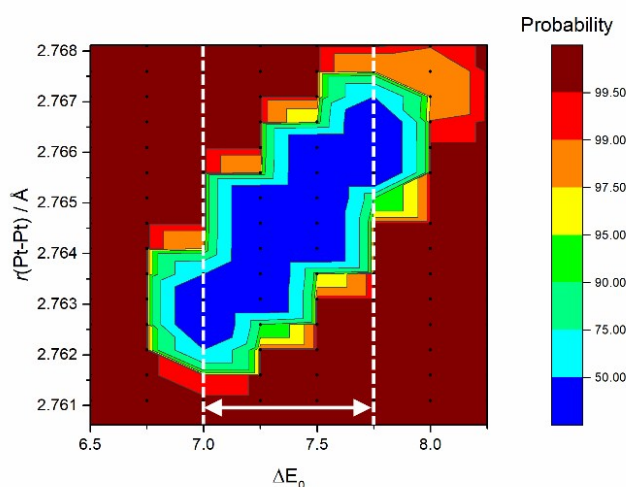


Figure S10. Correlation between $r(\text{Pt-Pt})$ and ΔE_0 for the Pt-foil and determination of the error in ΔE_0 using the F-test

8.0 eV have values higher than or equal to 95 %. This results in an error of ± 0.5 eV for ΔE_0 as determined on the Pt foil

We estimate the possible error due to changes during the measurements to be another ± 0.5 eV and end up with an error of ± 1 eV for ΔE_0 .

This error is used to determine the errors in $r(\text{Pt-Pt})$ and $r(\text{Pt-Co})$ for the various samples. Analogous to the procedure above, we varied ΔE_0 and $r(\text{Pt-Pt})$ or $r(\text{Pt-Co})$ for the samples, while optimizing all other fit parameters. The errors in $r(\text{Pt-Pt})$ are defined by the region of fits for which we can not reject the null hypothesis at the 95 % level or higher. But because we have determined ΔE_0 as $7.5 \text{ eV} \pm 1 \text{ eV}$ these are the only allowed values for ΔE_0 .

The resulting errors are shown in Table 2 in the paper and Table S2 in the Supporting Information. While there are only four fit parameters for the pure Pt samples [ΔE_0 , $r(\text{Pt-Pt})$, $N(\text{Pt-Pt})$ and $\sigma^2(\text{Pt-Pt})$] there are seven fit parameters for the Co-containing samples [ΔE_0 , $r(\text{Pt-Pt})$, $N(\text{Pt-Pt})$, $\sigma^2(\text{Pt-Pt})$, $r(\text{Pt-Co})$, $N(\text{Pt-Co})$ and $\sigma^2(\text{Pt-Co})$]. This leads to smaller F-values for the Co-containing samples and consequently, to larger errors.

For PtCoN ac, AuPtCoN bc and AuPtCoN ac the least squares fitting algorithm compensates very small or large values of $r(\text{Pt-Co})$ by making $\sigma^2(\text{Pt-Co})$ very large and/or making $N(\text{Pt-Co})$ negative. Neither of these is physically reasonable and the errors were determined for fits that do not show these issues.

Correlation between N and σ^2

In order to understand the correlation between N and σ^2 in more detail it is instructive to look at the change of coordination number N and R-factor as a function of σ^2 . Figure S11 shows a graph plotting $N(\text{Pt-Co})$ and the R-factor against $\sigma^2(\text{Pt-Co})$ for the PtCoN ac sample. This sample is chosen here to exemplify the correlation between N and σ^2 because the simple EXAFS fitting described in the paper yielded the largest value for $\sigma^2(\text{Pt-Co})$ for this sample (see Table 2). This plot was generated by fixing $\sigma^2(\text{Pt-Co})$ to values between 0.005 \AA^2 and 0.030 \AA^2 and optimizing $\sigma^2(\text{Pt-Pt})$, $N(\text{Pt-Pt})$, $N(\text{Pt-Co})$, $r(\text{Pt-Pt})$ and $r(\text{Pt-Co})$. Over this range, $N(\text{Pt-Co})$ increases from ~ 0.5 at $\sigma^2(\text{Pt-Co}) = 0.005 \text{ \AA}^2$ to ~ 5.5 at $\sigma^2(\text{Pt-Co}) = 0.030 \text{ \AA}^2$. The R-factor is largest at $\sigma^2(\text{Pt-Co}) = 0.005 \text{ \AA}^2$ with ~ 1.75 %. Between $\sigma^2(\text{Pt-Co}) = 0.018 \text{ \AA}^2$ and $\sigma^2(\text{Pt-Co}) = 0.030 \text{ \AA}^2$ the R-factor is between 1.1 % and 1.2 % while $N(\text{Pt-Co})$ varies between ~ 2.5 and ~ 5.5 . This correlation clearly results in physically unreasonable values for N and σ^2 . For example, the PtCoN ac sample has a very high value of $\sigma^2(\text{Pt-Co}) = 0.0231$ and

correspondingly, the total number of nearest neighbors around platinum,

$N_{\text{total}} = N(\text{Pt-Pt}) + N(\text{Pt-Co})$, is larger than 12.

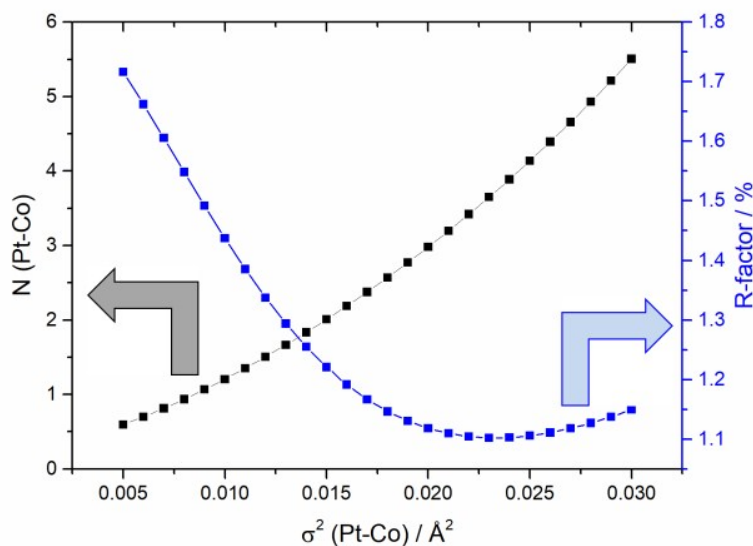


Figure S11. Number of Co atoms around Pt, $N(\text{Pt-Co})$, and quality of fit, R-factor, obtained from EXAFS fitting; the Debye-Waller factor $\sigma^2(\text{Pt-Co})$ was fixed to the values indicated on the x-axis while $\sigma^2(\text{Pt-Pt})$, $N(\text{Pt-Pt})$, $N(\text{Pt-Co})$, $r(\text{Pt-Pt})$ and $r(\text{Pt-Co})$ were optimized

2D Mapping – Systematic Variation of $\sigma^2(\text{Pt-Pt})$ and $\sigma^2(\text{Pt-Co})$

To systematically study the correlation between N and σ^2 for both scattering paths we performed what we call 2D-mapping: $\sigma^2(\text{Pt-Pt})$ and $\sigma^2(\text{Pt-Co})$ are set to fixed values and varied in steps of 0.001 \AA^2 and $N(\text{Pt-Pt})$, $N(\text{Pt-Co})$, $r(\text{Pt-Pt})$ and $r(\text{Pt-Co})$ are optimized. The results of this can be visualized by plotting one of the fit-parameters as a function of $\sigma^2(\text{Pt-Pt})$ and $\sigma^2(\text{Pt-Co})$. Instead of one of the four fit parameters, the R-factor or a parameter derived from the fit parameters, as will be described below, can also be plotted. Every dot marked on the contour plots in Figures S12 to S62 corresponds to one EXAFS fit. The lowest R-factors in the 2D-mapping are obtained for the values of $\sigma^2(\text{Pt-Pt})$ and $\sigma^2(\text{Pt-Co})$ closest to the values obtained in the simple EXAFS analysis, as is to be expected. While the R-factor increases significantly when increasing or decreasing $\sigma^2(\text{Pt-Pt})$ by more than 0.001 \AA^2 , a wide range of values of $\sigma^2(\text{Pt-Co})$ corresponds to fits with only a moderate increase in the R-factor. This matches the errors obtained from the least squares fitting algorithm used in the simple EXAFS analysis, see Table 2.

2D-Filtering

In the following analysis a set of criteria will be used to filter the fits in the 2D-mapping. The criteria are selected to filter out physically unreasonable or statistically insignificant EXAFS fits. The resulting, filtered set of EXAFS fits for each sample is used to calculate the variance of the Pt/Co-ratio around Pt, $\delta(\text{Pt/Co}_{\text{EXAFS}})$, and the variance of the total number of nearest neighbors, $\delta(N_{\text{total,EXAFS}})$. These two numbers are used in the model building analysis for normalization in the formula calculating the reliability factors for the comparisons, R_{comp} .

It should be noted that the Pt/Co- coordination number ratio around Pt is defined as $N(\text{Pt-Pt})/N(\text{Pt-Co})$. This should not be confused with the Pt/Co-ratio over the entire cluster.

In the model building analysis, both values occur. The Pt/Co-ratio around Pt is used to compare the structural models with the EXAFS fits while the Pt/Co-ratio over the entire molecule is used to make conclusions about the resulting structural models for the NPs.

The first filter-criterion used is a limit on the total number of nearest neighbours around platinum, $N_{\text{total}} = N(\text{Pt-Pt}) + N(\text{Pt-Co})$. Only fits with $9 \leq N_{\text{total}} \leq 12$ are allowed to pass this filter. The upper bound of 12 is very straightforward, it corresponds to the number of nearest neighbors in a closest packed structure. 9, on the other hand, is the number of nearest neighbor in a (111) terrace site of the fcc lattice, i.e. three atoms on-top of the central atom are removed. While there will be some Pt atoms in sites with less than nine nearest neighbors, i.e. corner or edge sites, (100) terrace sites and single Pt adatoms, other Pt atoms will be below the surface of the nanoparticle and thus have twelve nearest neighbors, so that nine nearest neighbors should be a reasonable lower limit for the average number of nearest neighbors.

The second filter-criterion imposes a limit on the acceptable R-factor. All fits with $R > 2 \cdot R_{\text{min}}$, where R_{min} is the smallest R-factor out of all the fits, are removed by this filter.

The third filter-criterion is based on the Pt/Co-ratio (around Pt) and uses the Pt/Co-ratios obtained with STEM-EDS (over the entire particle) (see Table 1). If the nanoparticles are (partially) segregated, e.g. if there is a Pt-shell, the Pt/Co-ratio around platinum, determined from EXAFS analysis and calculated as $N(\text{Pt-Pt})/N(\text{Pt-Co})$, should be larger than that from STEM-EDS, since the STEM-EDS Pt/Co-ratios are determined over the entire nanoparticle. If there is no order in a nanoparticle, i.e. the different elements are randomly distributed, the Pt/Co-ratio around Pt, as determined through EXAFS analysis, should be the same as the

overall Pt/Co-ratio of a particle, as measured by STEM-EDS. Only if the nanoparticle has an ordered arrangement of Pt and Co can there be a Pt/Co-ratio around Pt that is lower than the average Pt/Co-ratio over the whole particle, but XRD measurements did not indicate any crystallinity of the NPs. [3] In order to account for the error in the Pt/Co-ratio determined by STEM-EDS the third filter-criterion removes all fits with Pt/Co-ratios around Pt smaller than the value measured with STEM-EDS minus the associated error as given in Table 1.

The fourth and final criterion in the filtering of the 2D-mapping results is that $\sigma^2(\text{Pt-Co})$ has to be 0.005 \AA^2 or larger. This is the value obtained on a Pt₉Co reference sample which has a Pt fcc structure with every tenth Pt atom replaced by Co. The static disorder of the Pt-Co bond length in nanoparticles with Pt in various different positions within the nanoparticle as well as different sizes of nanoparticles should be larger than that in a well ordered fcc lattice, even if the Co atoms in that lattice are randomly distributed.

Contour plots showing the R-factor, Pt/Co-ratio around Pt and nearest neighbor number N_{total} as a function of $\sigma^2(\text{Pt-Pt})$ and $\sigma^2(\text{Pt-Co})$ as well as the results of the various filter criteria for PtCo, PtCoN and AuPtCoN nanoparticles before and after conditioning are shown in Figures S12 to S62s.

[3] Takahashi, S.; Takahashi, N.; Todoroki, N.; Wadayama, T. Dealloying of Nitrogen-Introduced Pt–Co Alloy Nanoparticles: Preferential Core–Shell Formation with Enhanced Activity for Oxygen Reduction Reaction. *ACS Omega*, **2016**, 1(6), 1247–1252.

<https://doi.org/10.1021/acsomega.6b00412>

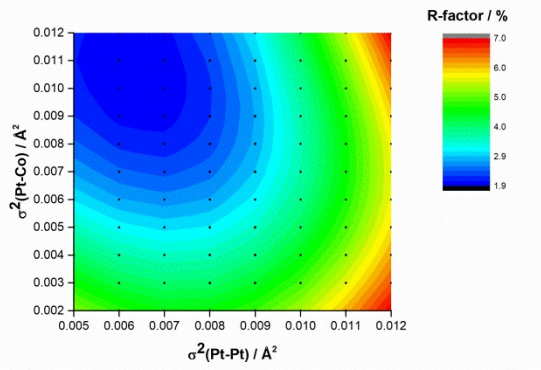


Figure S12. Contour plot showing the R-factor as a function of $\sigma^2(\text{Pt-Pt})$ and $\sigma^2(\text{Pt-Co})$; **PtCo bc** sample

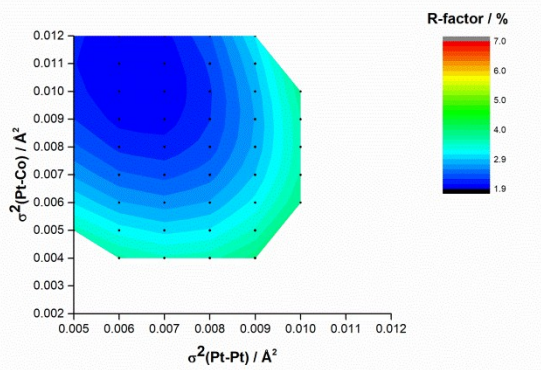


Figure S13. Contour plot showing the R-factor as a function of $\sigma^2(\text{Pt-Pt})$ and $\sigma^2(\text{Pt-Co})$; **PtCo bc** sample; filtered with the condition $R \leq 2 * R_{\min}$

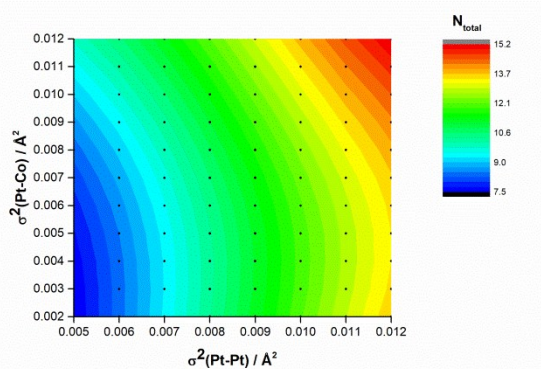


Figure S14. Contour plot showing the average number of nearest neighbours around Pt, N_{total} , as a function of $\sigma^2(\text{Pt-Pt})$ and $\sigma^2(\text{Pt-Co})$; **PtCo bc** sample

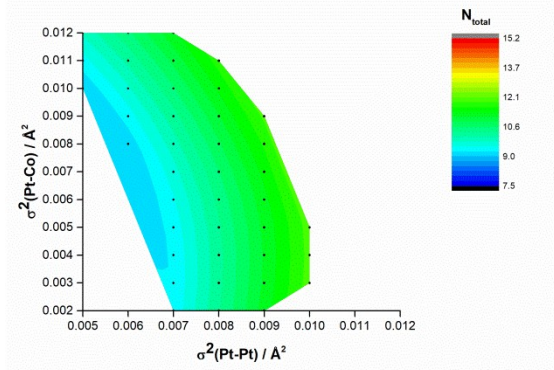


Figure S15. Contour plot showing the average number of nearest neighbours around Pt, N_{total} , as a function of $\sigma^2(\text{Pt-Pt})$ and $\sigma^2(\text{Pt-Co})$; **PtCo bc** sample; filtered with the condition $9 \leq N_{\text{total}} \leq 12$

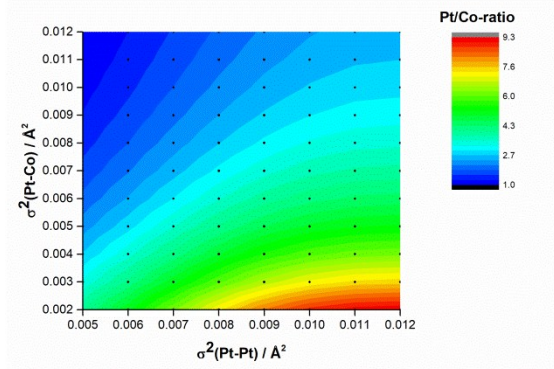


Figure S16. Contour plot showing the Pt/Co-ratio around Pt, $N(\text{Pt-Pt})/N(\text{Pt-Co})$, as a function of $\sigma^2(\text{Pt-Pt})$ and $\sigma^2(\text{Pt-Co})$; **PtCo bc** sample

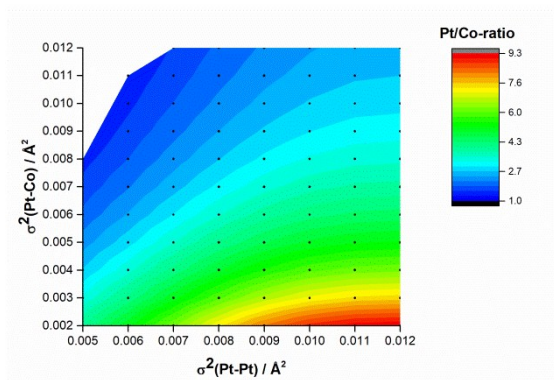


Figure S17. Contour plot showing the Pt/Co-ratio around Pt, $N(\text{Pt-Pt})/N(\text{Pt-Co})$, as a function of $\sigma^2(\text{Pt-Pt})$ and $\sigma^2(\text{Pt-Co})$; **PtCo bc** sample; filtered with the condition $\text{Pt/Co} \geq \text{Pt/Co}_{\text{STEM}}$

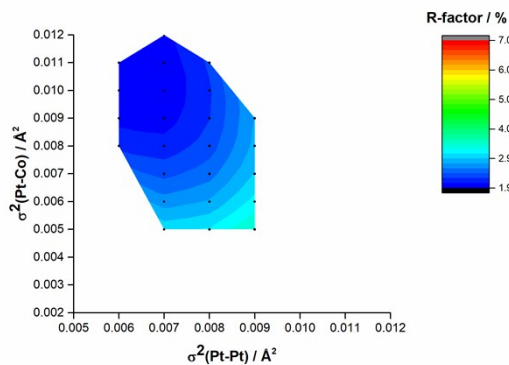


Figure S18. Contour plot showing the R-factor as a function of $\sigma^2(\text{Pt-Pt})$ and $\sigma^2(\text{Pt-Co})$; **PtCo bc** sample; filtered with all 4 filter criteria

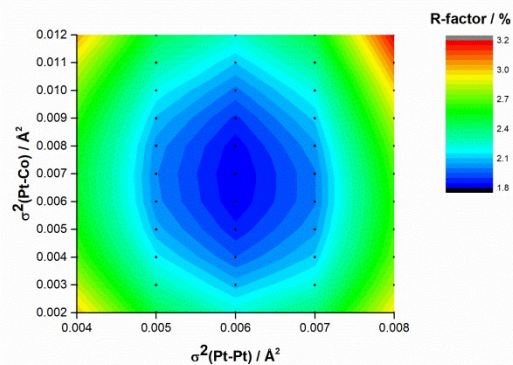


Figure S21. Contour plot showing the R-factor as a function of $\sigma^2(\text{Pt-Pt})$ and $\sigma^2(\text{Pt-Co})$; **PtCo ac** sample

Note: The maximum R-factor in Figure S29 is less than two times the best R-factor, thus, no plot filtered by $R \leq 2 * R_{\min}$ is shown

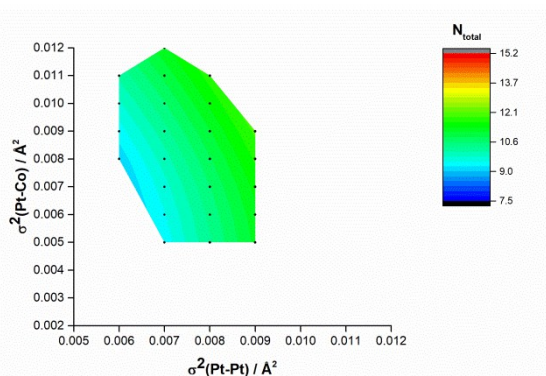


Figure S19. Contour plot showing the average number of nearest neighbours around Pt, N_{total} , as a function of $\sigma^2(\text{Pt-Pt})$ and $\sigma^2(\text{Pt-Co})$; **PtCo bc** sample; filtered with all 4 filter criteria

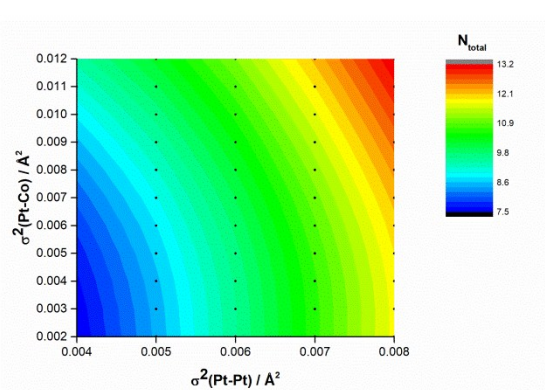


Figure S22. Contour plot showing the average number of nearest neighbours around Pt, N_{total} , as a function of $\sigma^2(\text{Pt-Pt})$ and $\sigma^2(\text{Pt-Co})$; **PtCo ac** sample

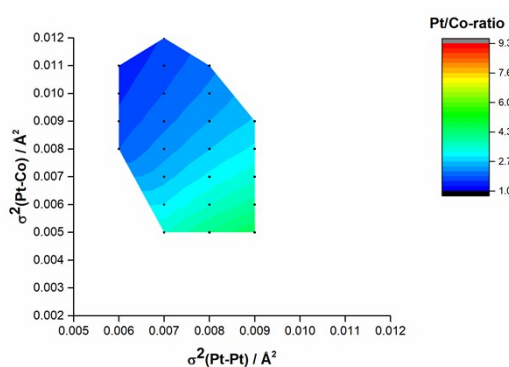


Figure S20. Contour plot showing the Pt/Co-ratio around Pt, $N(\text{Pt-Pt})/N(\text{Pt-Co})$, as a function of $\sigma^2(\text{Pt-Pt})$ and $\sigma^2(\text{Pt-Co})$; **PtCo bc** sample; filtered with all 4 filter criteria

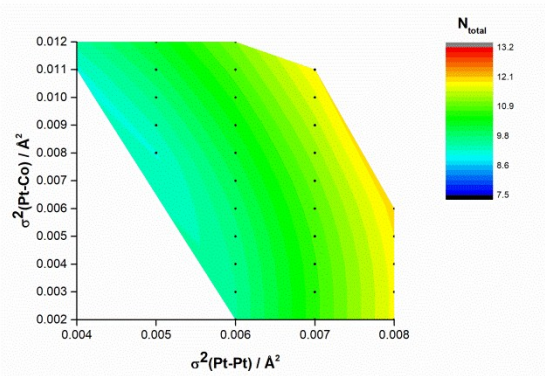


Figure S23. Contour plot showing the average number of nearest neighbours around Pt, N_{total} , as a function of $\sigma^2(\text{Pt-Pt})$ and $\sigma^2(\text{Pt-Co})$; **PtCo ac** sample; filtered with the condition $9 \leq N_{\text{total}} \leq 12$

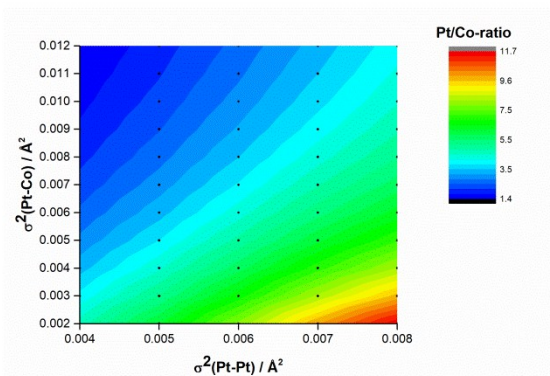


Figure S24. Contour plot showing the Pt/Co-ratio around Pt, $N(\text{Pt-Pt})/N(\text{Pt-Co})$, as a function of $\sigma^2(\text{Pt-Pt})$ and $\sigma^2(\text{Pt-Co})$; **PtCo ac** sample

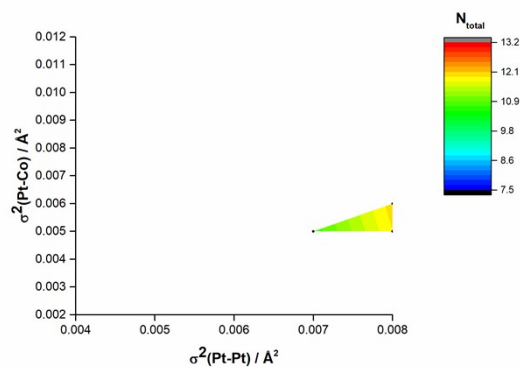


Figure S27. Contour plot showing the average number of nearest neighbours around Pt, N_{total} , as a function of $\sigma^2(\text{Pt-Pt})$ and $\sigma^2(\text{Pt-Co})$; **PtCo ac** sample; filtered with all 4 filter criteria

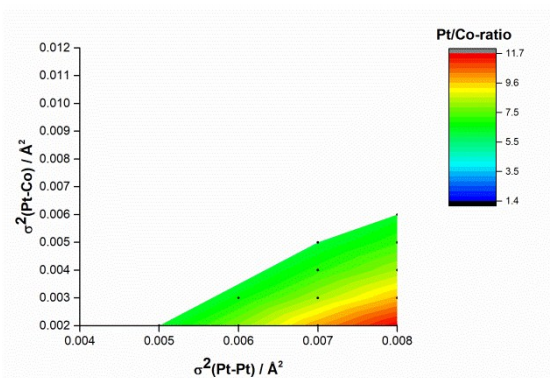


Figure S25. Contour plot showing the Pt/Co-ratio around Pt, $N(\text{Pt-Pt})/N(\text{Pt-Co})$, as a function of $\sigma^2(\text{Pt-Pt})$ and $\sigma^2(\text{Pt-Co})$; **PtCo ac** sample; filtered with the condition $\text{Pt/Co} \geq \text{Pt/Co}_{\text{STEM}}$

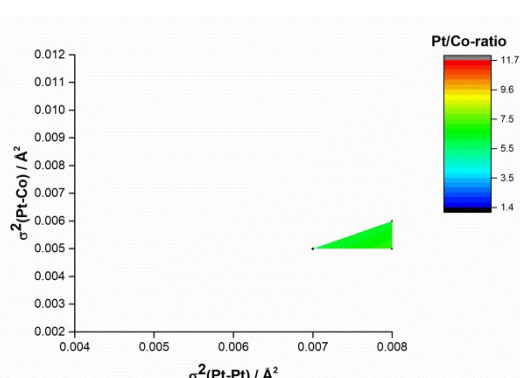


Figure S28. Contour plot showing the Pt/Co-ratio around Pt, $N(\text{Pt-Pt})/N(\text{Pt-Co})$, as a function of $\sigma^2(\text{Pt-Pt})$ and $\sigma^2(\text{Pt-Co})$; **PtCo ac** sample; filtered with all 4 filter criteria

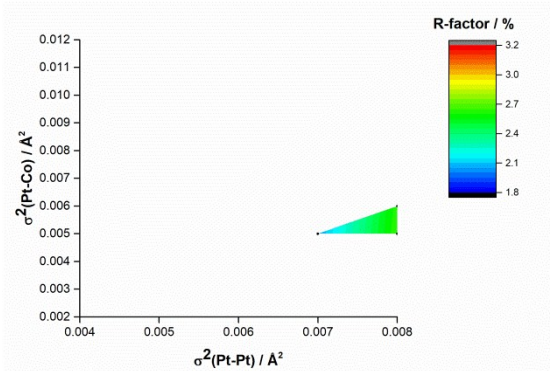


Figure S26. Contour plot showing the R-factor as a function of $\sigma^2(\text{Pt-Pt})$ and $\sigma^2(\text{Pt-Co})$; **PtCo ac** sample; filtered with all 4 filter criteria

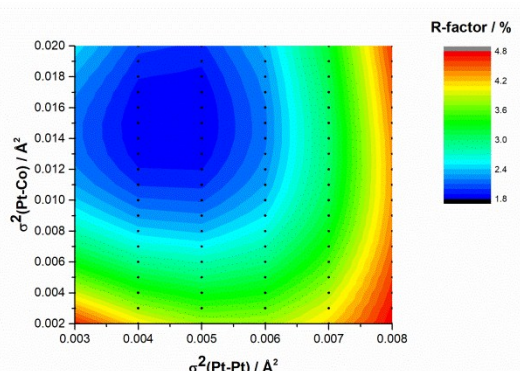


Figure S29. Contour plot showing the R-factor as a function of $\sigma^2(\text{Pt-Pt})$ and $\sigma^2(\text{Pt-Co})$; **PtCoN bc** sample

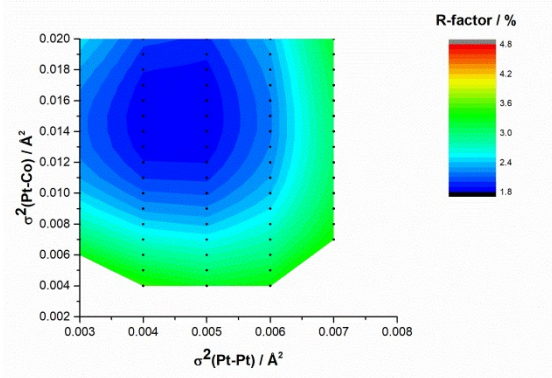


Figure S30. Contour plot showing the R-factor as a function of $\sigma^2(\text{Pt-Pt})$ and $\sigma^2(\text{Pt-Co})$; **PtCoN bc** sample; filtered with the condition $R \leq 2 * R_{\min}$

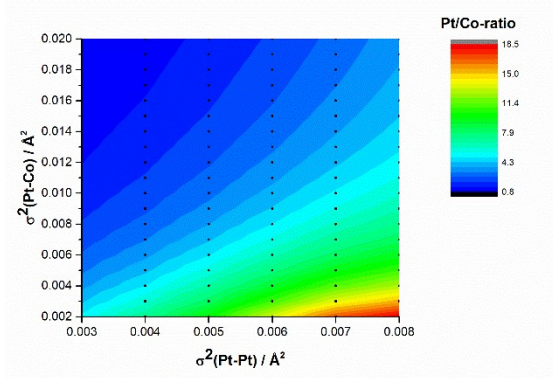


Figure S33. Contour plot showing the Pt/Co-ratio around Pt, $N(\text{Pt-Pt})/N(\text{Pt-Co})$, as a function of $\sigma^2(\text{Pt-Pt})$ and $\sigma^2(\text{Pt-Co})$; **PtCoN bc** sample

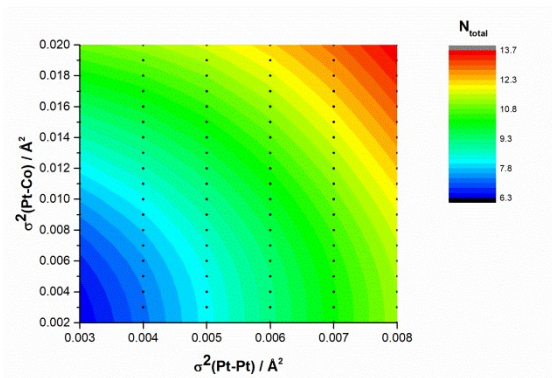


Figure S31. Contour plot showing the average number of nearest neighbours around Pt, N_{total} , as a function of $\sigma^2(\text{Pt-Pt})$ and $\sigma^2(\text{Pt-Co})$; **PtCoN bc** sample

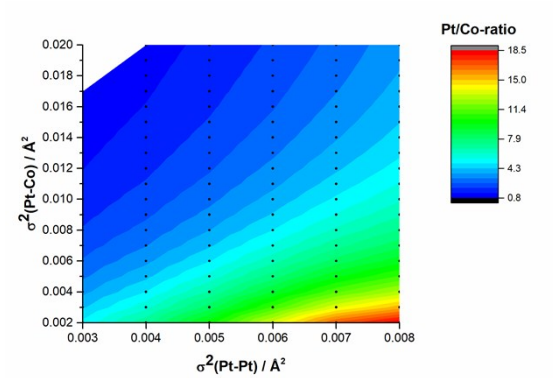


Figure S34. Contour plot showing the Pt/Co-ratio around Pt, $N(\text{Pt-Pt})/N(\text{Pt-Co})$, as a function of $\sigma^2(\text{Pt-Pt})$ and $\sigma^2(\text{Pt-Co})$; **PtCoN bc** sample; filtered with the condition $\text{Pt/Co} \geq \text{Pt/Co}_{\text{STEM}}$

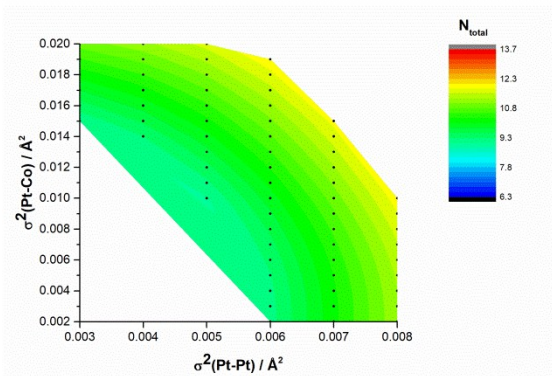


Figure S32. Contour plot showing the average number of nearest neighbours around Pt, N_{total} , as a function of $\sigma^2(\text{Pt-Pt})$ and $\sigma^2(\text{Pt-Co})$; **PtCoN bc** sample; filtered with the condition $9 \leq N_{\text{total}} \leq 12$

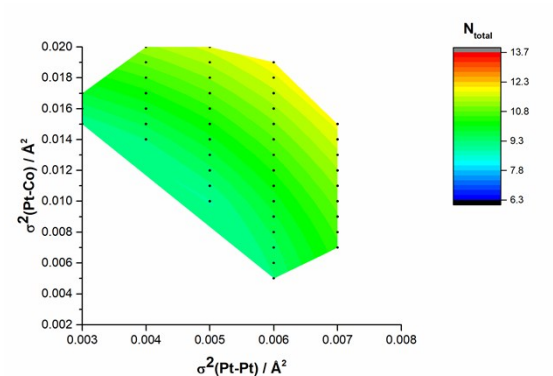


Figure S35. Contour plot showing the average number of nearest neighbours around Pt, N_{total} , as a function of $\sigma^2(\text{Pt-Pt})$ and $\sigma^2(\text{Pt-Co})$; **PtCoN bc** sample; filtered with all 4 filter criteria

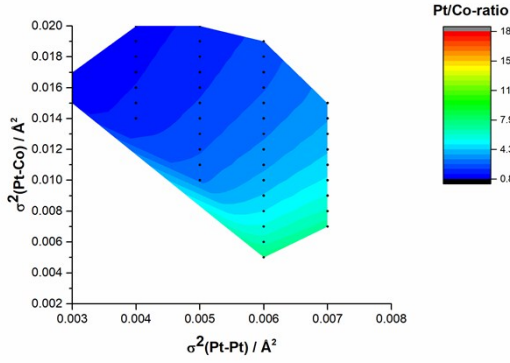


Figure S36. Contour plot showing the Pt/Co-ratio around Pt, $N(\text{Pt-Pt})/N(\text{Pt-Co})$, as a function of $\sigma^2(\text{Pt-Pt})$ and $\sigma^2(\text{Pt-Co})$; **PtCoN bc** sample; filtered with all 4 filter criteria

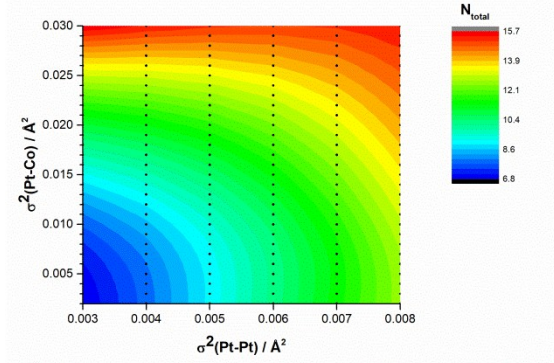


Figure S39. Contour plot showing the average number of nearest neighbours around Pt, N_{total} , as a function of $\sigma^2(\text{Pt-Pt})$ and $\sigma^2(\text{Pt-Co})$; **PtCoN ac** sample

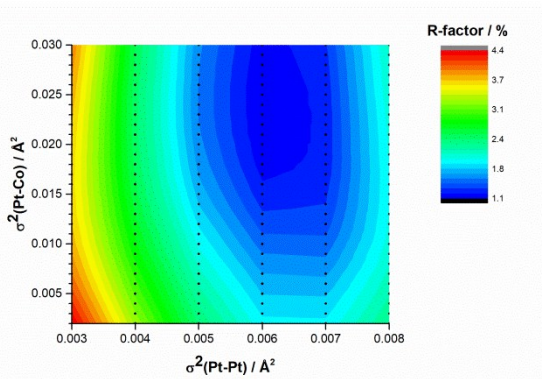


Figure S37. Contour plot showing the R-factor as a function of $\sigma^2(\text{Pt-Pt})$ and $\sigma^2(\text{Pt-Co})$; **PtCoN ac** sample

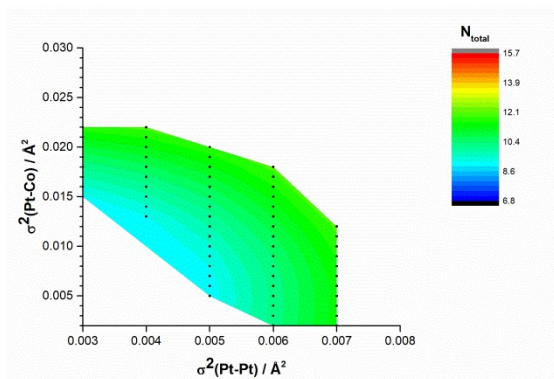


Figure S40. Contour plot showing the average number of nearest neighbours around Pt, N_{total} , as a function of $\sigma^2(\text{Pt-Pt})$ and $\sigma^2(\text{Pt-Co})$; **PtCoN ac** sample; filtered with the condition $9 \leq N_{\text{total}} \leq 12$

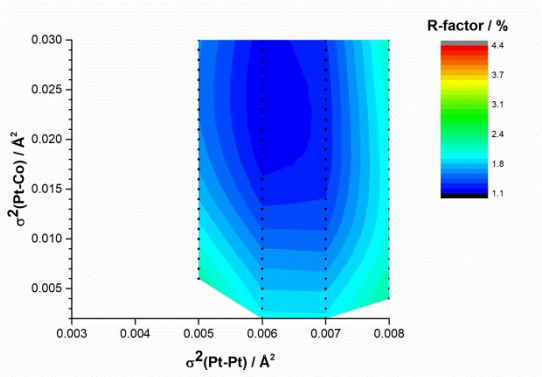


Figure S38. Contour plot showing the R-factor as a function of $\sigma^2(\text{Pt-Pt})$ and $\sigma^2(\text{Pt-Co})$; **PtCoN ac** sample; filtered with the condition $R \leq 2 \cdot R_{\text{min}}$

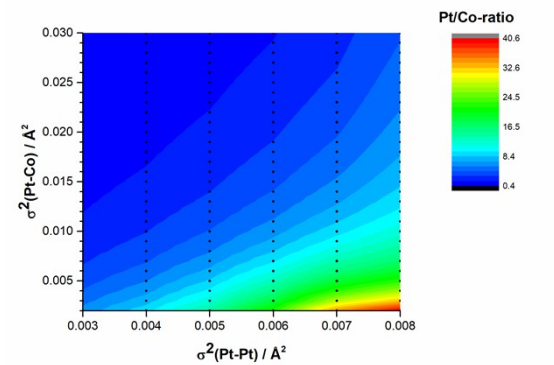


Figure S41. Contour plot showing the Pt/Co-ratio around Pt, $N(\text{Pt-Pt})/N(\text{Pt-Co})$, as a function of $\sigma^2(\text{Pt-Pt})$ and $\sigma^2(\text{Pt-Co})$; **PtCoN ac** sample

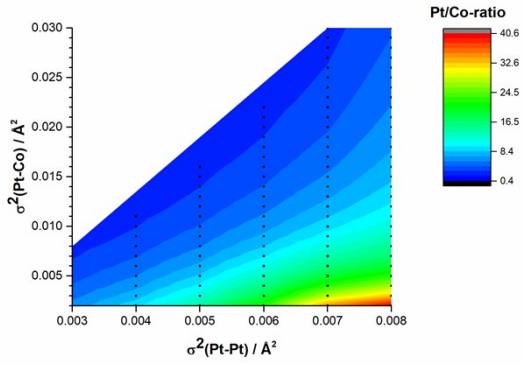


Figure S42. Contour plot showing the Pt/Co-ratio around Pt, $N(\text{Pt-Pt})/N(\text{Pt-Co})$, as a function of $\sigma^2(\text{Pt-Pt})$ and $\sigma^2(\text{Pt-Co})$; **PtCoN ac** sample; filtered with the condition $\text{Pt/Co} \geq \text{Pt/Co}_{\text{STEM}}$

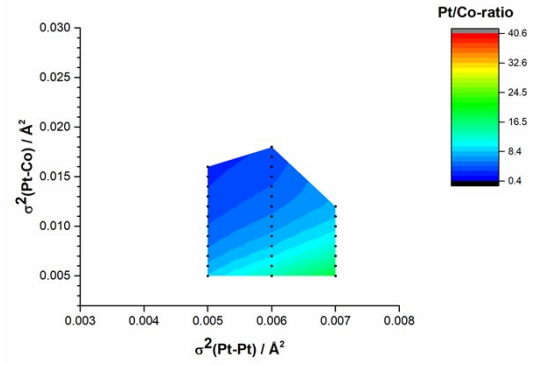


Figure S45. Contour plot showing the Pt/Co-ratio around Pt, $N(\text{Pt-Pt})/N(\text{Pt-Co})$, as a function of $\sigma^2(\text{Pt-Pt})$ and $\sigma^2(\text{Pt-Co})$; **PtCoN ac** sample; filtered with all 4 filter criteria

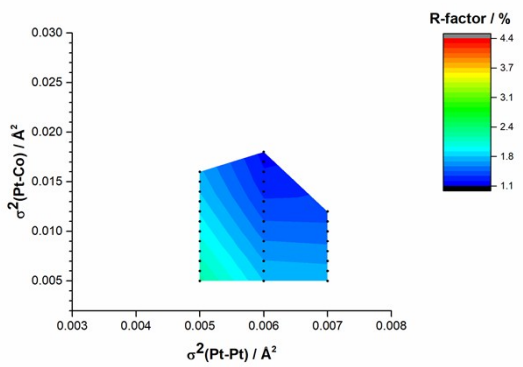


Figure S43. Contour plot showing the R-factor as a function of $\sigma^2(\text{Pt-Pt})$ and $\sigma^2(\text{Pt-Co})$; **PtCoN ac** sample; filtered with all 4 filter criteria

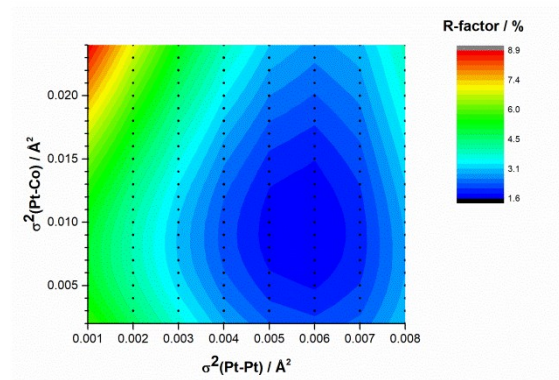


Figure S46. Contour plot showing the R-factor as a function of $\sigma^2(\text{Pt-Pt})$ and $\sigma^2(\text{Pt-Co})$; **AuPtCoN bc** sample

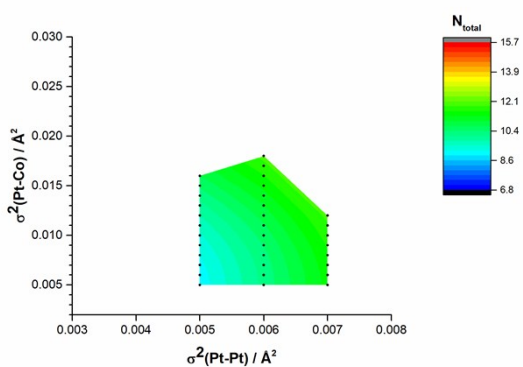


Figure S44. Contour plot showing the average number of nearest neighbours around Pt, N_{total} , as a function of $\sigma^2(\text{Pt-Pt})$ and $\sigma^2(\text{Pt-Co})$; **PtCoN ac** sample; filtered with all 4 filter criteria

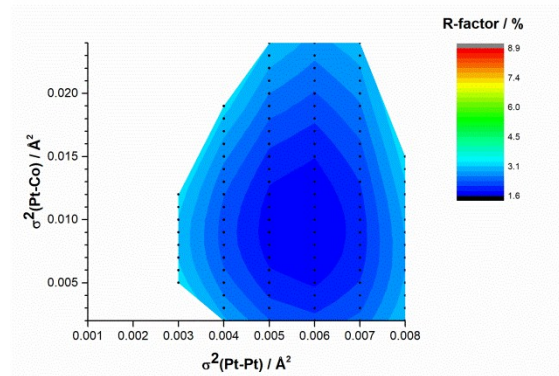


Figure S47. Contour plot showing the R-factor as a function of $\sigma^2(\text{Pt-Pt})$ and $\sigma^2(\text{Pt-Co})$; **AuPtCoN bc** sample; filtered with the condition $R \leq 2 * R_{\text{min}}$

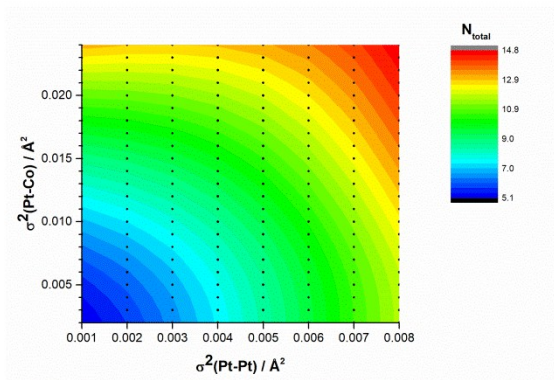


Figure S48. Contour plot showing the average number of nearest neighbours around Pt, N_{total} , as a function of $\sigma^2(\text{Pt-Pt})$ and $\sigma^2(\text{Pt-Co})$; **AuPtCoN bc** sample

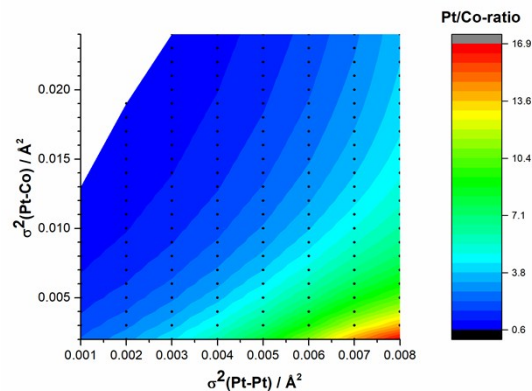


Figure S51. Contour plot showing the Pt/Co-ratio around Pt, $N(\text{Pt-Pt})/N(\text{Pt-Co})$, as a function of $\sigma^2(\text{Pt-Pt})$ and $\sigma^2(\text{Pt-Co})$; **AuPtCoN bc** sample; filtered with the condition $\text{Pt/Co} \geq \text{Pt/Co}_{\text{STEM}}$

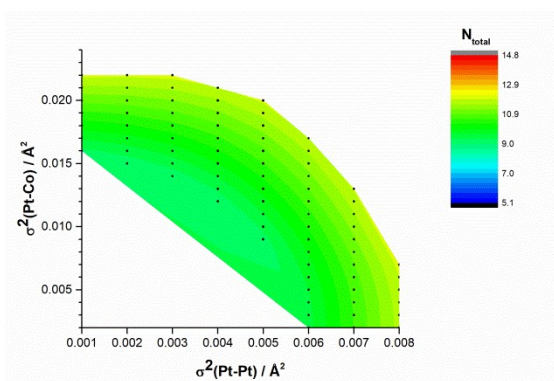


Figure S49. Contour plot showing the average number of nearest neighbours around Pt, N_{total} , as a function of $\sigma^2(\text{Pt-Pt})$ and $\sigma^2(\text{Pt-Co})$; **AuPtCoN bc** sample; filtered with the condition $9 \leq N_{\text{total}} \leq 12$

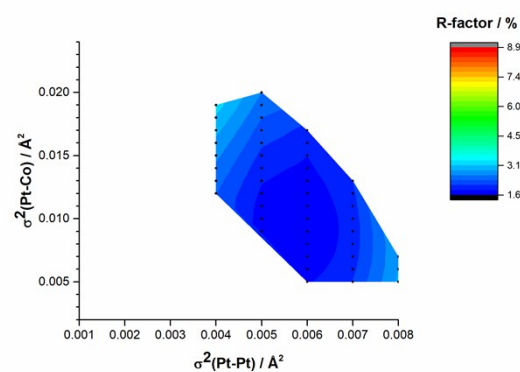


Figure S52. Contour plot showing the R-factor as a function of $\sigma^2(\text{Pt-Pt})$ and $\sigma^2(\text{Pt-Co})$; **AuPtCoN bc** sample; filtered with all 4 filter criteria

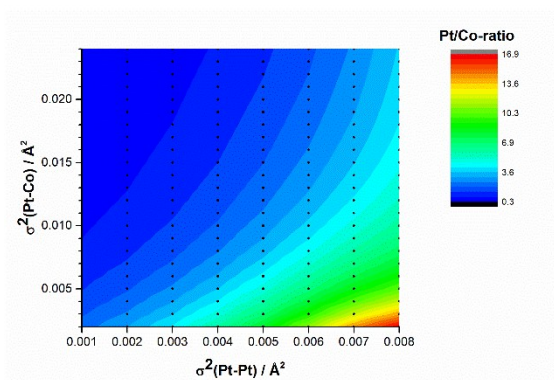


Figure S50. Contour plot showing the Pt/Co-ratio around Pt, $N(\text{Pt-Pt})/N(\text{Pt-Co})$, as a function of $\sigma^2(\text{Pt-Pt})$ and $\sigma^2(\text{Pt-Co})$; **AuPtCoN bc** sample

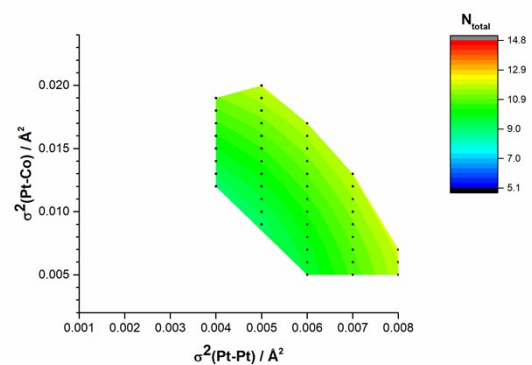


Figure S53. Contour plot showing the average number of nearest neighbours around Pt, N_{total} , as a function of $\sigma^2(\text{Pt-Pt})$ and $\sigma^2(\text{Pt-Co})$; **AuPtCoN bc** sample; filtered with all 4 filter criteria

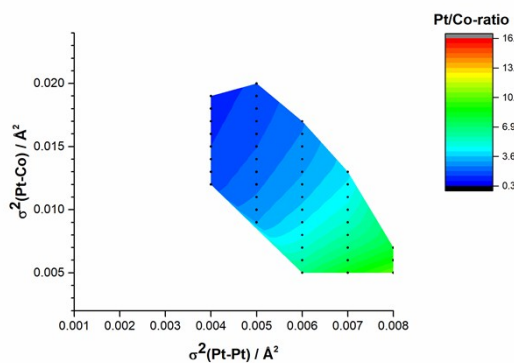


Figure S54. Contour plot showing the Pt/Co-ratio around Pt, $N(\text{Pt-Pt})/N(\text{Pt-Co})$, as a function of $\sigma^2(\text{Pt-Pt})$ and $\sigma^2(\text{Pt-Co})$; **AuPtCoN bc** sample; filtered with all 4 filter criteria

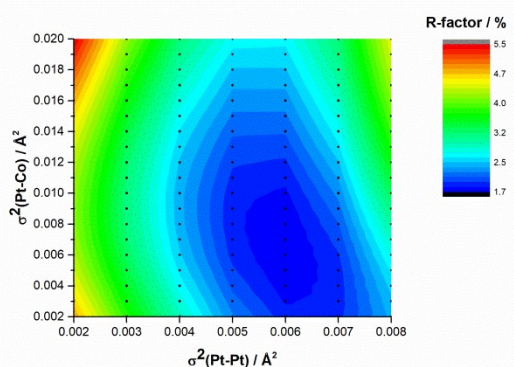


Figure S55. Contour plot showing the R-factor as a function of $\sigma^2(\text{Pt-Pt})$ and $\sigma^2(\text{Pt-Co})$; **AuPtCoN ac** sample

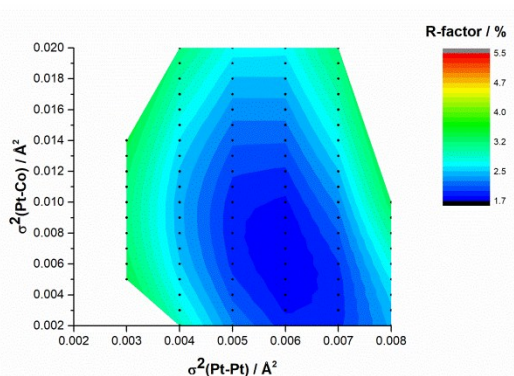


Figure S56. Contour plot showing the R-factor as a function of $\sigma^2(\text{Pt-Pt})$ and $\sigma^2(\text{Pt-Co})$; **AuPtCoN ac** sample; filtered with the condition $R \leq 2 * R_{\min}$

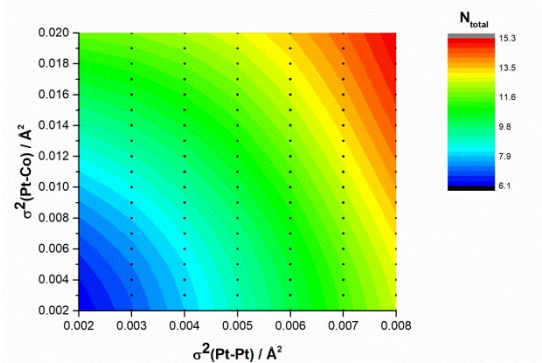


Figure S57. Contour plot showing the average number of nearest neighbours around Pt, N_{total} , as a function of $\sigma^2(\text{Pt-Pt})$ and $\sigma^2(\text{Pt-Co})$; **AuPtCoN ac** sample

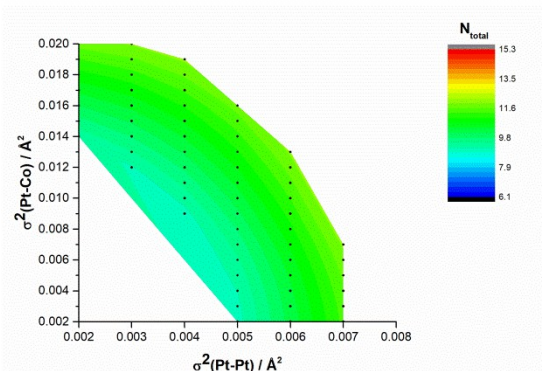


Figure S58. Contour plot showing the average number of nearest neighbours around Pt, N_{total} , as a function of $\sigma^2(\text{Pt-Pt})$ and $\sigma^2(\text{Pt-Co})$; **AuPtCoN ac** sample; filtered with the condition $9 \leq N_{\text{total}} \leq 12$

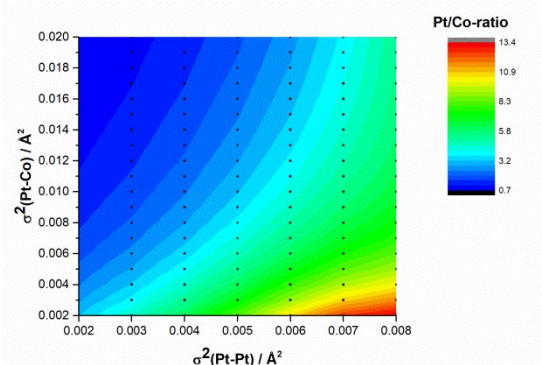


Figure S59. Contour plot showing the Pt/Co-ratio around Pt, $N(\text{Pt-Pt})/N(\text{Pt-Co})$, as a function of $\sigma^2(\text{Pt-Pt})$ and $\sigma^2(\text{Pt-Co})$; **AuPtCoN ac** sample

Note: The minimum Pt/Co-ratio within the error, as determined by STEM-EDS, is smaller than the smallest value in **Figure S59**. Thus, no plot filtered by Pt/Co-ratio is shown

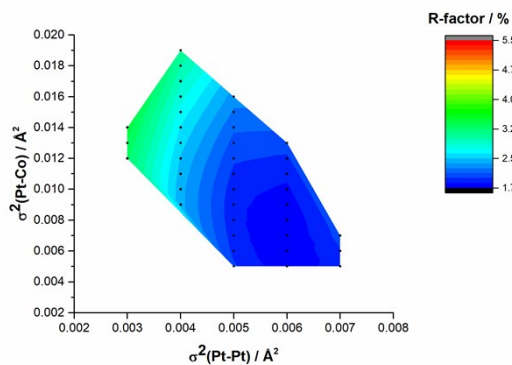


Figure S60. Contour plot showing the R-factor as a function of $\sigma^2(\text{Pt-Pt})$ and $\sigma^2(\text{Pt-Co})$; AuPtCoN ac sample; filtered with all 4 filter criteria

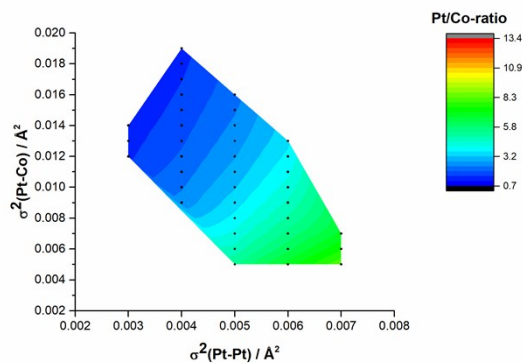


Figure S62. Contour plot showing the Pt/Co-ratio around Pt, $N(\text{Pt-Pt})/N(\text{Pt-Co})$, as a function of $\sigma^2(\text{Pt-Pt})$ and $\sigma^2(\text{Pt-Co})$; AuPtCoN ac sample; filtered with all 4 filter criteria

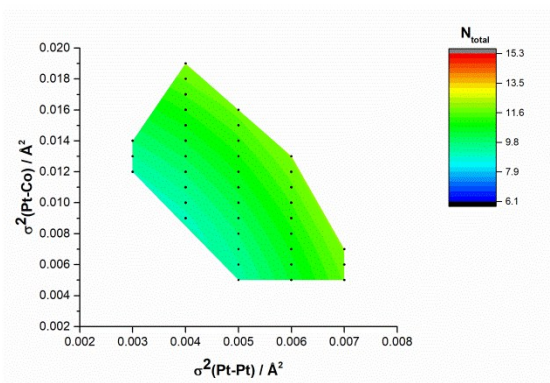


Figure S61. Contour plot showing the average number of nearest neighbours around Pt, N_{total} , as a function of $\sigma^2(\text{Pt-Pt})$ and $\sigma^2(\text{Pt-Co})$; AuPtCoN ac sample; filtered with all 4 filter criteria

Additional explanations about the computer program used to generate the structural models for the nanoparticles

In the construction of the spherical particles the bulk structure of Pt, with a Pt-Pt bond length of 2.775 Å, was used. The bond length is not important for our analysis as we compare nearest neighbor numbers and ratios of Pt/Co around Pt [$N(\text{Pt-Pt})/N(\text{Pt-Co})$] between structural models and EXAFS fits.

In the next step Pt atoms are replaced with Co atoms to generate a particle with the desired Pt/Co-ratio (over the entire molecule), Pt-shell thickness and Co-core thickness. After taking these three parameters as input, the script then replaces Pt atoms with Co until the Pt/Co-ratio in the structural model becomes smaller than or equal to the defined Pt/Co-ratio. In this

replacement, Pt atoms in the central region, corresponding to the Co-core, are replaced first, if the Co-core radius is larger than 0 Å. Pt atoms in the shell defined through the Pt-shell thickness are exempt from replacement. Within these constraints the Pt atom to be replaced is selected at random in each case.

N atoms are ignored for the analytical part of the model building, since they are not relevant for the EXAFS analysis or its comparison with the structural models. For the visualizations shown in Figure 7 one nitrogen atom was added to one of the interstitial sites next to each cobalt atom, hinting at the formation of CoN in the N-containing NPs.

Finally, for the AuPtCoN structural models, Au atoms are added in fcc lattice positions on the surface. Since preferential occupation of low-coordination sites is expected [4], the script put Au atoms in the lowest coordinated sites first.

For each sample, the Pt/Co-ratio was varied in steps of 0.1 within the error determined by STEM-EDS. The thickness of the Pt-shell was varied between 0 Å (no shell) and 10 Å in 1 Å steps, the radius of the Co-core was varied between 0 Å (no Co-core) and 10 Å in 1 Å steps. For the PtCo ac nanoparticles not all combinations of Pt-shell and Co-core thickness could be realized due to the large Pt/Co-ratio. The number of Au atoms for the models of gold containing nanoparticles was varied between 0 and 800 in steps of 100. Table S1 gives an overview over the numbers of models generated in this way.

In the final step of the program, two output files are generated for each model structure. One output file is in xyz- and contains the structure of the model in Cartesian coordinates. The other output file describes the statistics of the nanoparticle and includes the two parameters that are used in the comparison between models and EXAFS fits: the Pt/Co-ratio around Co and N_{total} . The parameters are calculated for a structure by calculating them for each Pt atom in the structure and averaging over the values for all Pt atoms.

[4] Takahashi, S.; Chiba, H.; Kato, T.; Endo, S.; Hayashi, T.; Todoroki, N.; Wadayama, T. Oxygen reduction reaction activity and structural stability of Pt–Au nanoparticles prepared by arc-plasma deposition. *Phys. Chem. Chem. Phys.*, **2015**, 17(28), 18638–18644.

<https://doi.org/10.1039/C5CP02048D>

Table S1. Minimum and maximum Pt/Co-ratios used in the model building, numbers of structural models and numbers of comparisons between structural models and EXAFS fits before and after filtering as well as resulting numbers of EXAFS fits

Sample	Pt/Co-ratio		Number of Models	Number of Comparisons		Number of EXAFS fits
	minimum	maximum		unfiltered	filtered	
PtCo bc	1.4	2.0	306	26928	5931	30
PtCo ac	5.9	9.8	3422	391326	2981	10
PtCoN bc	1.0	2.0	1595	181831	20964	53
PtCoN ac	2.6	3.4	968	108417	16616	37
AuPtCoN bc	0.6	1.4	5184	856568	177827	68
AuPtCoN ac	0.6	2.3	9900	1316700	215423	81

The Pt/Co-ratios in Table S1 give the minimum and maximum values used in the construction of the structural models for the respective samples. The number of models results from the combination of Pt/Co-ratios with various different types of structures (core-shell, completely random, different shell thicknesses as discussed in the paper and above). Each of the models is compared with each of the EXAFS fits obtained in the 2D-mapping for the corresponding sample. This leads to the number of comparisons (unfiltered). After applying the filtering described in the paper to these comparisons, the number of comparisons (filtered) remains. These are the comparisons that pass the filtering and are used to calculate the resulting EXAFS fit parameters and model parameters. The last column, the number of EXAFS fits (filtered), shows how many different EXAFS fits are represented in the comparisons that pass the model building filtering.

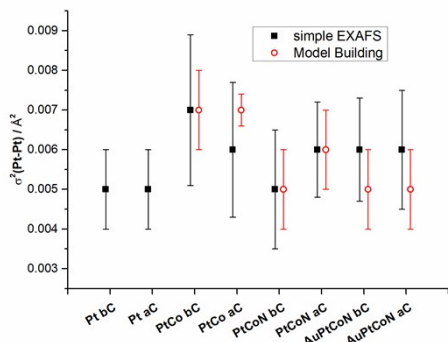


Figure S63. $\sigma^2(\text{Pt-Pt})$ with error bars obtained with simple EXAFS fitting (black squares) and model building (red open circles).

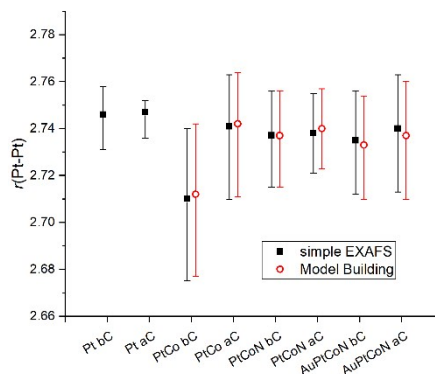


Figure S65. $r(\text{Pt-Pt})$ with error bars obtained with simple EXAFS fitting (black squares) and model building (red open circles).

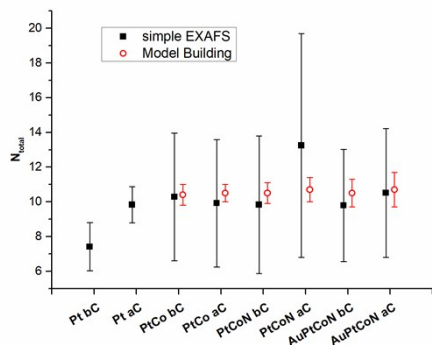


Figure S64. Total number of nearest neighbors around Pt, N_{total} , with error bars obtained with simple EXAFS fitting (black squares) and model building (red open circles).

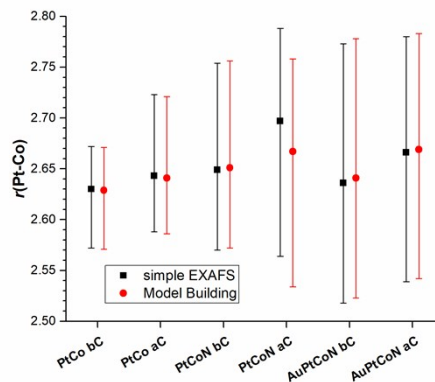


Figure S66. $r(\text{Pt-Co})$ with error bars obtained with simple EXAFS fitting (black squares) and model building (red open circles).

Table S2. Overview over EXAFS parameters resulting from the filtered model building comparisons with standard deviations; R-factors are the average value over all comparisons that pass the model building filtering for the respective sample; the errors for r are taken from the error calculation performed for simple EXAFS described above

	Path	$\sigma^2 / \text{\AA}^2$	$r / \text{\AA}$	N_{total}	$N_{\text{Pt-Pt}}/N_{\text{Pt-Co}}$ ratio	R-factor
PtCo bc	Pt-Pt	0.007 ± 0.001	2.71 ± 0.04	10.4 ± 0.6	2.2 ± 0.8	2.3 %
	Pt-Co	0.009 ± 0.002	2.63 ± 0.06			
PtCo ac	Pt-Pt	0.007 ± 0.0004	2.74 ± 0.03	10.5 ± 0.5	7.7 ± 1.3	2.2 %
	Pt-Co	0.003 ± 0.001	2.61 ± 0.08			
PtCoN bc	Pt-Pt	0.005 ± 0.001	2.74 ± 0.02	10.5 ± 0.6	2.3 ± 1.3	2.2 %
	Pt-Co	0.015 ± 0.003	2.65 ± 0.11			
PtCoN ac	Pt-Pt	0.006 ± 0.001	2.74 ± 0.02	10.7 ± 0.7	4.9 ± 2.6	1.6 %
	Pt-Co	0.013 ± 0.003	2.67 ± 0.13			
AuPtCoN bc	Pt-Pt	0.005 ± 0.001	2.73 ± 0.02	10.5 ± 0.8	2.0 ± 1.3	2.1 %
	Pt-Co	0.014 ± 0.003	2.64 ± 0.14			
AuPtCoN ac	Pt-Pt	0.005 ± 0.001	2.74 ± 0.03	10.7 ± 1.0	2.9 ± 1.5	2.3 %
	Pt-Co	0.012 ± 0.004	2.67 ± 0.14			

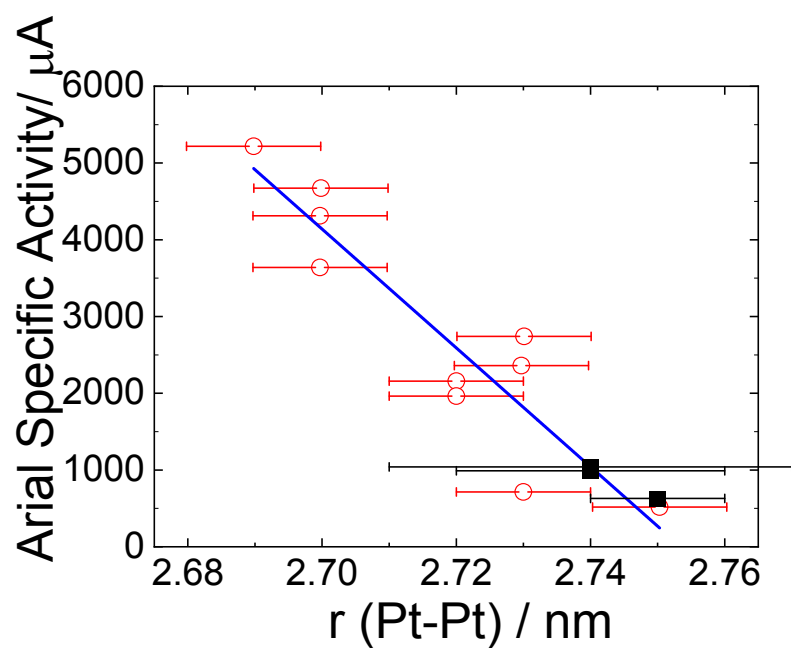


Figure S67. Correlation between area specific activity and Pt-Pt bond distances of Pt M alloy particles on C powder prepared in the previously reported way (red open circle) and those on HOPG prepared by APD method (this work) (black filled squares).